



## Article

# Pyrido[2',1':2,3]imidazo[4,5-c]isoquinolin-5-amines as Potential Cytotoxic Agents against Human Neuroblastoma

Zahira Tber<sup>1</sup>, Mohammed Loubidi<sup>1</sup> , Jabrane Jouha<sup>1</sup>, Ismail Hdoufane<sup>2</sup> , Mümin Alper Erdogan<sup>3</sup> , Luciano Saso<sup>4</sup> , Güliz Armagan<sup>5,\*</sup> and Sabine Berteina-Raboin<sup>1,\*</sup>

- <sup>1</sup> Institut de Chimie Organique et Analytique ICOA, Université d'Orléans-Pôle de Chimie, UMR CNRS 7311, Rue de Chartres-BP 6759, CEDEX 2, 45067 Orléans, France; tber\_zahira@yahoo.com (Z.T.); m.loubidi@gmail.com (M.L.); jabranejouha@gmail.com (J.J.)
- <sup>2</sup> Laboratory of Molecular Chemistry, Faculty of Sciences Semlalia, Cadi Ayyad University, Marrakech BP 2390, Morocco; i.hdoufane@gmail.com
- <sup>3</sup> Department of Physiology, School of Medicine, İzmir Katip Çelebi University, Izmir 35620, Turkey; alpero86@gmail.com
- <sup>4</sup> Department of Physiology and Pharmacology Vittorio Erspamer, Sapienza University of Rome, P. le Aldo Moro 5, 00185 Rome, Italy; luciano.saso@uniroma1.it
- <sup>5</sup> Department of Biochemistry, Faculty of Pharmacy, Ege University, Bornova 35100, Turkey
- \* Correspondence: guliz.armagan@ege.edu.tr (G.A.); sabine.berteina-raboin@univ-orleans.fr (S.B.-R.); Tel.: +33-238-494-856 (S.B.-R.)



**Citation:** Tber, Z.; Loubidi, M.; Jouha, J.; Hdoufane, I.; Erdogan, M.A.; Saso, L.; Armagan, G.; Berteina-Raboin, S. Pyrido[2',1':2,3]imidazo[4,5-c]isoquinolin-5-amines as Potential Cytotoxic Agents against Human Neuroblastoma. *Pharmaceuticals* **2021**, *14*, 750. <https://doi.org/10.3390/ph14080750>

Academic Editor: Pascal Marchand

Received: 16 June 2021

Accepted: 24 July 2021

Published: 30 July 2021

**Publisher's Note:** MDPI stays neutral with regard to jurisdictional claims in published maps and institutional affiliations.



**Copyright:** © 2021 by the authors. Licensee MDPI, Basel, Switzerland. This article is an open access article distributed under the terms and conditions of the Creative Commons Attribution (CC BY) license (<https://creativecommons.org/licenses/by/4.0/>).

**Abstract:** We report herein the evaluation of various pyrido[2',1':2,3]imidazo[4,5-c]isoquinolin-5-amines as potential cytotoxic agents. These molecules were obtained by developing the multi-component Groebke–Blackburn–Bienaymé reaction to yield various pyrido[2',1':2,3]imidazo[4,5-c]quinolines which are isosteres of ellipticine whose biological activities are well established. To evaluate the anticancer potential of these pyrido[2',1':2,3]imidazo[4,5-c]isoquinolin-5-amine derivatives in the human neuroblastoma cell line, the cytotoxicity was examined using the WST-1 assay after 72 h drug exposure. A clonogenic assay was used to assess the ability of treated cells to proliferate and form colonies. Protein expressions (Bax, bcl-2, cleaved caspase-3, cleaved PARP-1) were analyzed using Western blotting. The colony number decrease in cells was 50.54%, 37.88% and 27.12% following exposure to compounds **2d**, **2g** and **4b** respectively at 10  $\mu$ M. We also show that treating the neuroblastoma cell line with these compounds resulted in a significant alteration in caspase-3 and PARP-1 cleavage.

**Keywords:** human neuroblastoma; PARP-1 inhibitors; anticancer drugs; pyrido[2',1':2,3]imidazo[4,5-c]isoquinolin-5-amines; antiproliferative activity

## 1. Introduction

Among the most common types of pediatric solid tumors, neuroblastoma is responsible for nearly 15% of pediatric cancer mortality [1]. Unfortunately, children at high risk show low survival rates despite rigorous treatment [1–4]. To fight against this, there are several different treatment strategies, including surgery, chemotherapy, radiation therapy, myeloablative therapy, stem cell transplantation, and immunotherapy. This treatment palette could be improved with alternative strategies including immunotherapy and novel anticancer drugs with limited adverse and side effects [5,6] (Figure 1). Research in this area with more targeted approaches remains necessary for patients with high-risk neuroblastoma. We describe herein the synthesis and the evaluation of pyrido[2',1':2,3]imidazo[4,5-c]isoquinolin-5-amine derivatives as potential anticancer agents in the human neuroblastoma cell line.

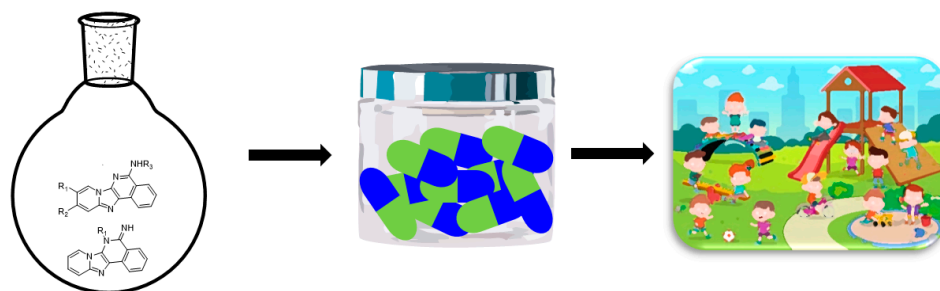
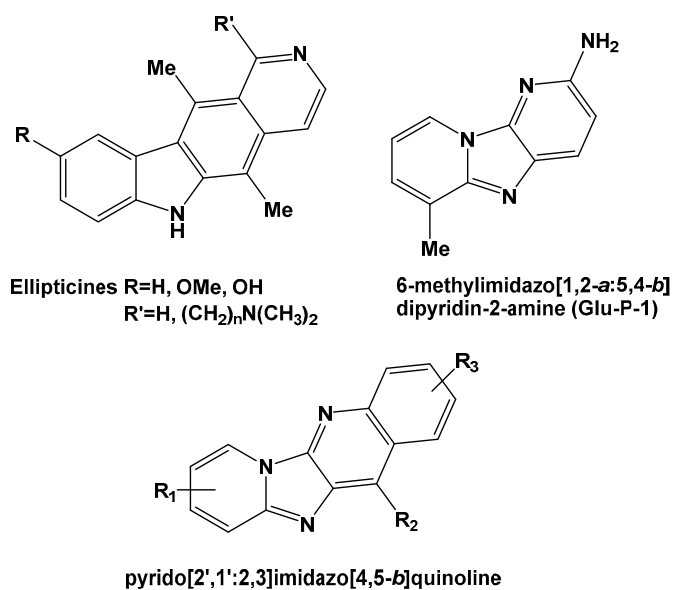
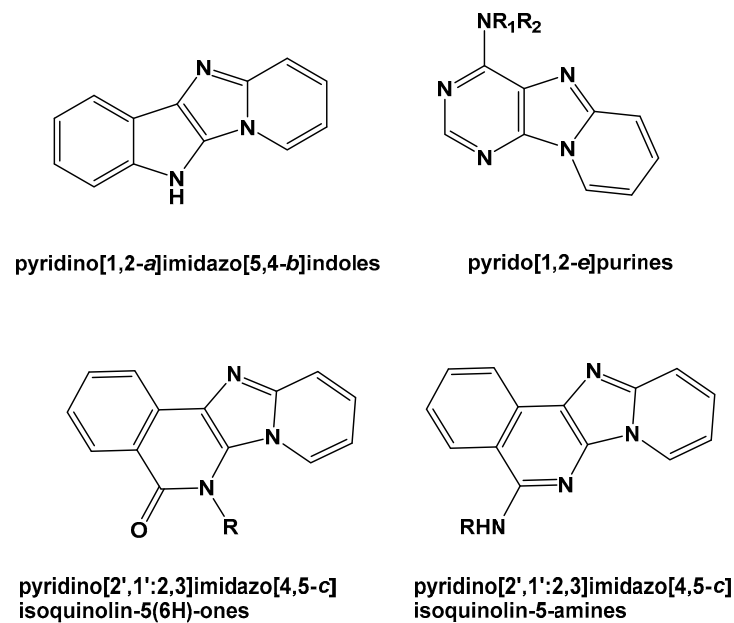


**Figure 1.** These potentially active molecules could become drug candidates for the protection of children and prevent pediatric cancer mortality.

Carcinogenesis increases as long as apoptosis does not occur in many cancer cells [7,8]. It is well known that malignantly transformed cells play a crucial role in the progress of cancer. As a cell death mechanism, apoptosis is very important to avoid the proliferation of these cells. Therefore, many proteins that are involved in the apoptotic pathway are considered as important targets for several anticancer drugs. The imidazo[1,2-*a*]heterocyclic scaffold is a prominent structural core system present in numerous biologically active compounds and possesses a wide range of biological activities. Many investigations revealed the anticancer potential of imidazo[1,2-*a*]heterocycle derivatives [9–14]. They have also been introduced as anti-inflammatory [15,16] and anti-tumor agents [17,18] and are active in the treatment of central nervous diseases [19]. Moreover, it has been reported that several drugs with an imidazo[1,2-*a*]pyridine scaffold such as zolpidem or alpidem can be used to treat insomnia or anxiety disorders [20,21]. The Pyrido[2',1':2,3]imidazo[4,5-*c*]quinolines are isosteres of ellipticine known to have various anti-cancer activities [22–26]. After studying their synthesis by the Groebke–Blackburn–Bienaymé MCR [27,28] Scheme 1, we were interested via the same kind of reaction to the synthesis of pyrido[2',1':2,3]imidazo[4,5-*c*]isoquinolin-5-amines Scheme 2 [29]. We evaluated the anticancer potential of these structures in the human neuroblastoma cell line, the cytotoxicity was examined using the WST-1 test after 72 h of exposure to drugs.



**Scheme 1.** Ellipticines and analogues.



**Scheme 2.** Example of fused imidazopyridines and pyrido [2',1':2,3]imidazo[4,5-c]isoquinolin-5-amines.

This work describes the synthesis, molecular docking results and evaluation of the anticancer potential of pyrido[2',1':2,3]imidazo[4,5-c]isoquinolin-5-amine derivatives in human neuroblastoma in a preclinical model. Furthermore, molecular modelling investigations were performed to suggest possible binding modes of these inhibitors inside the active site of the target protein (Figure 2).

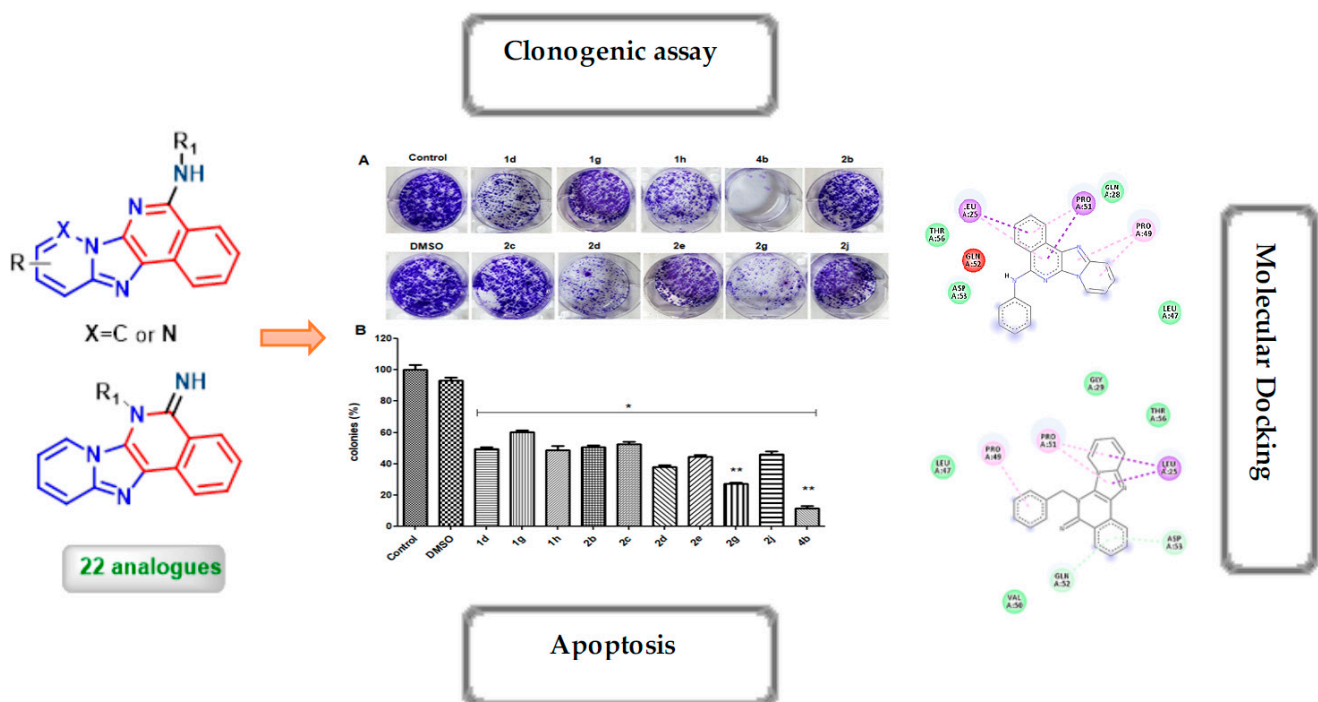
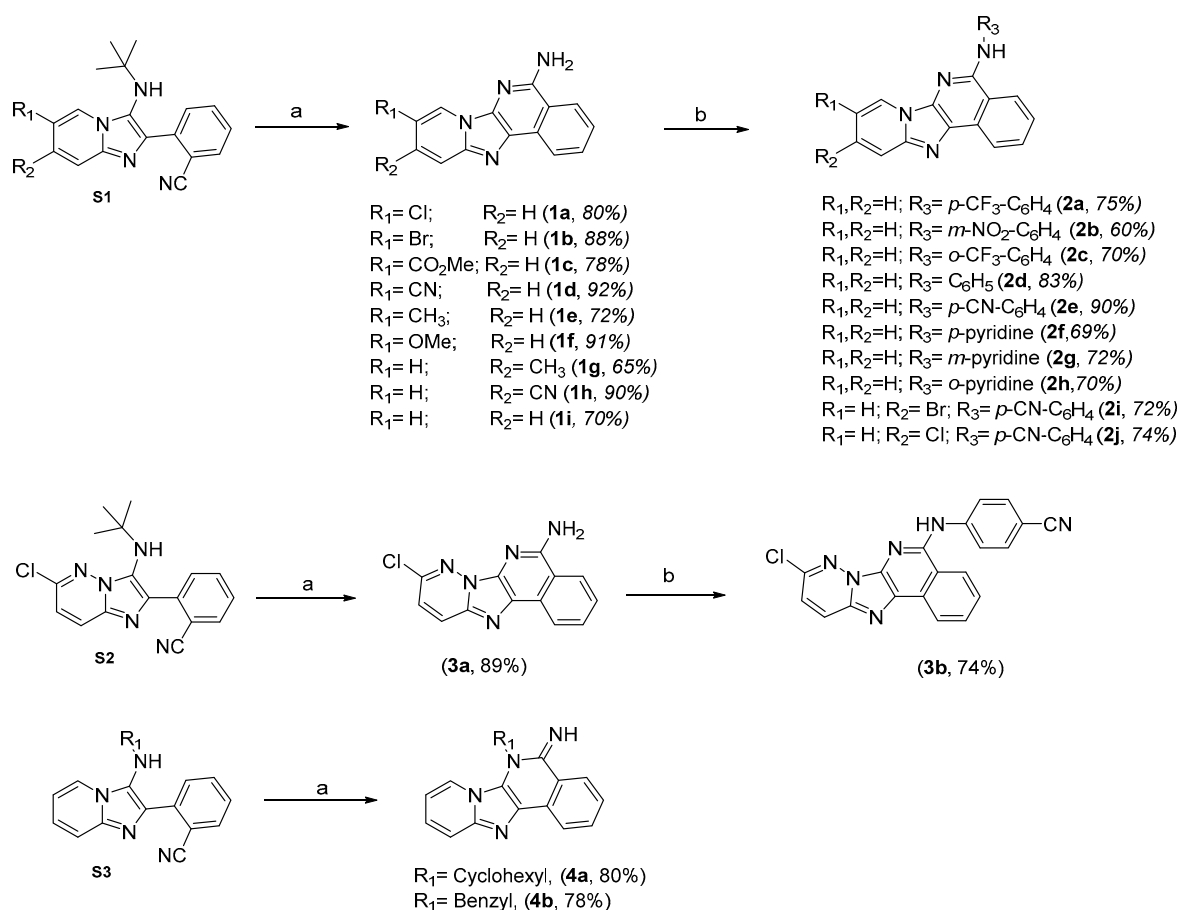


**Figure 2.** Scheme summarizing the results of this study. (A) Representative images of clonogenic assay in SH-SY5Y cells treated with the indicated drugs at 10  $\mu$ M. (B) Percentage of viable clones after drug treatments with respect to untreated cells. \*  $p < 0.01$  significant difference from control group, \*\*  $p < 0.01$  significant difference from other compounds.

## 2. Results and Discussion

### 2.1. Chemistry

The general synthetic route for the target compounds is outlined in Scheme 3. Compounds **1a–1i** were obtained from various products S1 that were obtained by a one-pot Groebke–Blackburn–Bienaymé MCR reaction according to our already published procedure [29] using 2-aminoheteroaryl, 2-formylbenzonitrile and *tert*-butylisocyanide in DCM at room temperature. During the N-deprotection step with a 1/1 mixture of DCM/TFA at room temperature, the electrophilic carbon of the cyano group underwent amine attack and cyclisation took place, leading to the pyrido[2',1':2,3]imidazo[4,5-*c*]isoquinolin-5-amines. To obtain the different substituted pyrido[2',1':2,3]imidazo[4,5-*c*]isoquinolin-5-amines **2a–2j** and **3a**, the synthetic strategy of the Buchwald reaction [30,31] was applied. Various aryl halides substituted in *para*, *meta* and *ortho* position were successfully introduced in good to excellent yields. Replacing *tert*-butyl by cyclohexyl and benzyl allowed us to synthesise novel imidazo[4,5-*c*]isoquinoline derivatives (**4a**, **4b**) with good yields via a one-step N-deprotection/cyclisation reaction.



**Scheme 3.** Synthetic route for various substituted pyridazo/pyrido[2',1':2,3]imidazo[4,5-*c*]isoquinolin-5-amines. Conditions: (a) TFA/DCM(1:1), rt; (b)  $R_2\text{-H}$ , (hetero)aryl halide,  $\text{Pd}(\text{OAc})_2$ , Xantphos,  $\text{Cs}_2\text{CO}_3$ , PhMe, 120 °C.

### 2.2. Biological Studies

#### 2.2.1. Cell Viability Studies

The cytotoxic potential of compounds was firstly evaluated in human neuroblastoma cell lines in terms of decrease in cell viability. WST-1 methods were used to evaluate the cytotoxicity of the synthesized compounds. The changes in cell viability after 72 h drug exposure are shown in Table 1. It was found that all the compounds tested, except **1d**, **1h**,

**2a**, **2f**, **2i**, **2j** and **3b**, showed moderate antiproliferative activity against the cancer cells. In particular, the IC<sub>50</sub> values of compounds **1g**, **2d** and **4b** were found to be less than 10  $\mu$ M.

**Table 1.** Cell viability analysis of newly synthesized compounds in human neuroblastoma cell lines. All values are means  $\pm$  SDs ( $n = 5$ ).

Compound	IC <sub>50</sub> ( $\mu$ M)	% Cell Viability $\pm$ S.D.			
		0.1 $\mu$ M	1 $\mu$ M	10 $\mu$ M	100 $\mu$ M
<b>1a</b>	30.92	79.26 $\pm$ 7.30	74.37 $\pm$ 3.07	56.05 $\pm$ 1.49	42.28 $\pm$ 3.54
<b>1b</b>	20.22	78.13 $\pm$ 7.12	82.00 $\pm$ 7.82	80.76 $\pm$ 17.03	2.82 $\pm$ 0.68
<b>1c</b>	63.57	73.13 $\pm$ 6.09	64.93 $\pm$ 8.65	59.36 $\pm$ 3.36	47.06 $\pm$ 2.76
<b>1d</b>	>100	67.87 $\pm$ 1.59	74.17 $\pm$ 1.80	68.67 $\pm$ 1.23	58.14 $\pm$ 5.16
<b>1e</b>	29.72	74.28 $\pm$ 7.46	76.26 $\pm$ 9.43	69.99 $\pm$ 5.20	32.25 $\pm$ 1.75
<b>1f</b>	62.75	95.60 $\pm$ 7.30	83.16 $\pm$ 2.45	61.48 $\pm$ 3.22	48.50 $\pm$ 1.59
<b>1g</b>	4.31	67.22 $\pm$ 2.46	77.39 $\pm$ 13.70	48.98 $\pm$ 2.88	2.8 $\pm$ 2.13
<b>1h</b>	>100	98.76 $\pm$ 18.97	88.84 $\pm$ 9.17	63.66 $\pm$ 3.69	77.20 $\pm$ 10.89
<b>2a</b>	>100	103.32 $\pm$ 7.22	124.52 $\pm$ 24.18	122.45 $\pm$ 3.75	53.93 $\pm$ 10.50
<b>2b</b>	75.51	89.66 $\pm$ 5.59	77.28 $\pm$ 6.50	58.54 $\pm$ 2.45	41.20 $\pm$ 6.35
<b>2c</b>	65.03	77.25 $\pm$ 0.46	73.04 $\pm$ 1.71	68.01 $\pm$ 6.44	42.65 $\pm$ 2.82
<b>2d</b>	9.68	79.99 $\pm$ 2.81	71.43 $\pm$ 1.99	69.37 $\pm$ 6.58	2.68 $\pm$ 0.78
<b>2e</b>	21.09	81.18 $\pm$ 2.57	76.57 $\pm$ 7.64	61.70 $\pm$ 3.10	32.39 $\pm$ 11.92
<b>2f</b>	>100	89.52 $\pm$ 10.33	83.36 $\pm$ 10.20	70.19 $\pm$ 4.08	52.03 $\pm$ 0.82
<b>2g</b>	20.54	96.81 $\pm$ 11.13	81.72 $\pm$ 2.09	59.98 $\pm$ 3.53	30.02 $\pm$ 3.13
<b>2h</b>	91.71	85.05 $\pm$ 8.52	77.79 $\pm$ 5.59	72.48 $\pm$ 4.91	45.71 $\pm$ 1.66
<b>2i</b>	>100	99.39 $\pm$ 5.10	82.60 $\pm$ 3.65	89.10 $\pm$ 8.44	85.14 $\pm$ 6.14
<b>2j</b>	>100	96.16 $\pm$ 17.53	82.43 $\pm$ 14.56	81.94 $\pm$ 8.51	109.05 $\pm$ 9.13
<b>3a</b>	43.51	98.72 $\pm$ 6.89	90.64 $\pm$ 6.24	68.55 $\pm$ 4.49	38.98 $\pm$ 2.26
<b>3b</b>	>100	79.29 $\pm$ 4.73	83.81 $\pm$ 2.62	85.39 $\pm$ 1.74	106.26 $\pm$ 10.35
<b>4a</b>	15.53	69.08 $\pm$ 5.18	72.08 $\pm$ 3.46	76.77 $\pm$ 8.51	17.89 $\pm$ 2.70
<b>4b</b>	1.68	73.29 $\pm$ 2.02	63.74 $\pm$ 5.20	27.16 $\pm$ 2.43	9.24 $\pm$ 2.60

The ability of cells to form colonies is crucial. The number of colonies was therefore counted 7 days after exposure to 10  $\mu$ M of drugs that were selected after the cell viability analyses (Figure 3). We found that exposure to compounds **2d**, **2g** and **4b** significantly diminished the number of clones per field as compared to cells from the control group ( $p < 0.01$ ), indicating the importance of further preclinical investigations.

### 2.2.2. Protein Analysis

Based on the results obtained by the clonogenic assay, further analyses were conducted for compounds **2d**, **2g** and **4b** at three different concentrations (1–100  $\mu$ M) in order to understand their possible roles in regulating protein levels including cleaved caspase 3, cleaved PARP, Bax and Bcl2, which are responsible for cell death. Results from the Western blot analysis showed that the treatment of SH-SY5Y cells with different concentrations of the selected compounds for 72 h upregulated some apoptotic proteins such as Bax, cleaved caspase-3 and cleaved PARP-1.

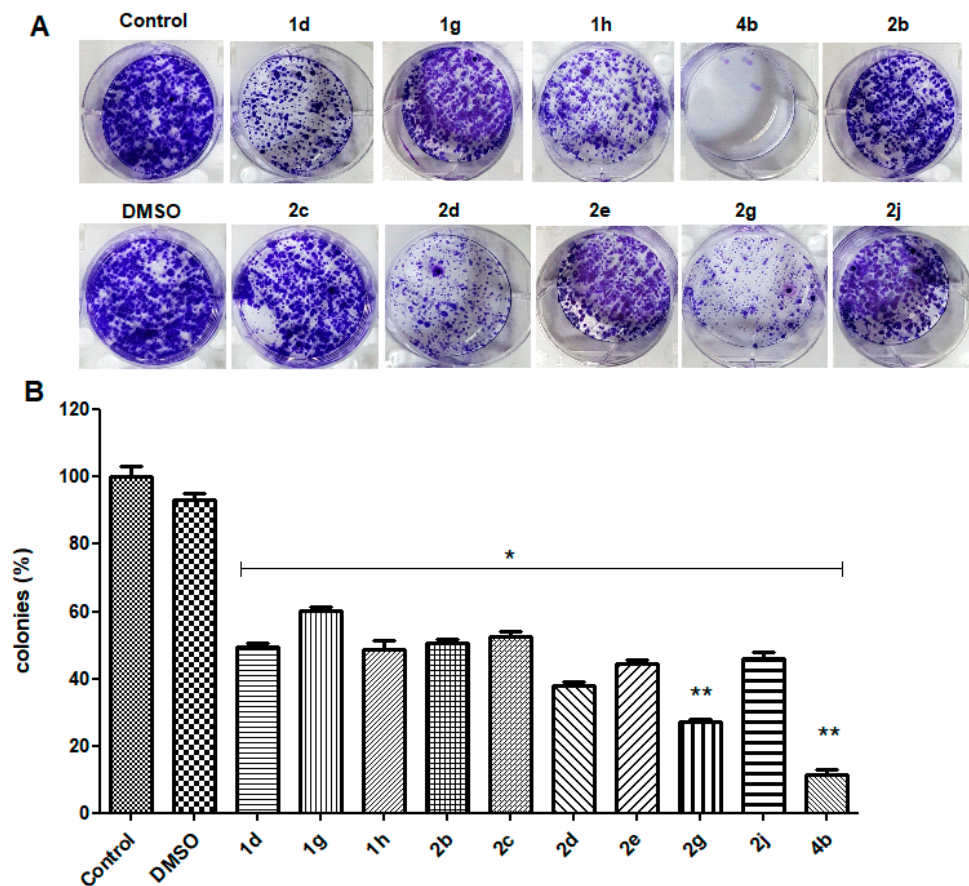


**Figure 3.** (A) Representative images of clonogenic assay in SH-SY5Y cells treated with the indicated drugs at 10  $\mu$ M. (B) Percentage of viable clones after drug treatments with respect to untreated cells. \*  $p < 0.01$  significant difference from control group, \*\*  $p < 0.01$  significant difference from other compounds.

The balance between Bax and bcl-2 controls cell apoptosis. As shown in Figure 4, increases in Bax protein levels in cells treated at higher concentrations were accompanied by concomitant decreases of Bcl-2 protein expression when compared to the control group (Figure 4,  $p < 0.05$ ), suggesting that the selected compounds have a regulatory potential for apoptosis by controlling the induction of mitochondrial dysfunction.

The activation of effector caspases, particularly caspase 3, plays an important role in the actual execution of apoptosis [32,33]. In our study, the results showed that these compounds have the potential to regulate activation of the caspase 3 enzyme in a dose-dependent manner. The exposure of SH-SY5Y cells to compounds (2d, 2g and 4b), at 10  $\mu$ M enhanced caspase-3 cleavage by 3.12, 4.62 and 3.79 fold, respectively (Figure 5) compared to the control group, thereby initiating the intrinsic apoptotic cascade.

One of several known cellular substrates of caspases is PARP-1. It is known that PARP-1 is involved in the prevention of DNA degradation and resistance to apoptosis. In recent studies, increased PARP-1 expression was shown to be associated with higher neuroblastoma stage and poor overall survival [34]. Thus, PARP-1 inhibitors are evaluated clinically for the treatment of brain tumors. However, the cleavage of PARP-1 by caspases is considered to be a hallmark of apoptosis [35] and caspase 3 is primarily responsible for the cleavage of this enzyme during programmed cell death [36]. In our study, the treatment of SH-SY5Y cells with compounds 2d, 2g and 4b at lower concentrations also led to the cleavage of PARP-1 when compared to the control group (Figure 5). Our data clearly indicated that the compounds activated the intrinsic caspase cascade leading to caspase-3 activation that resulted in PARP-1 cleavage in the neuroblastoma cell line. With

these Western Blot analyses, we addressed the question of whether the compounds in question can induce apoptotic cell death.

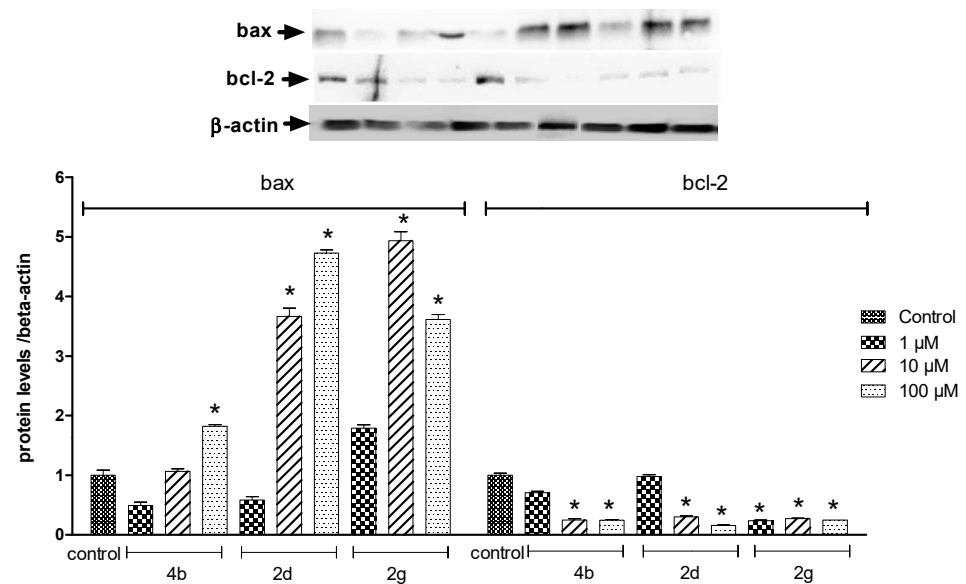


**Figure 4.** Changes in pro-apoptotic Bax and anti-apoptotic bcl-2 protein levels. Representative Western blots showing protein expressions of Bax and bcl-2 following the treatment of compounds 2d, 2g and 4b at three concentrations (1, 10 and 100  $\mu$ M). Graphs indicate the relative densitometric values of the proteins. Quantification of protein product was performed by densitometric scanning. Data were normalized by using the  $\beta$ -actin signal and are expressed as arbitrary densitometric units. Values are means SD;  $n = 5$  in each group. \*  $p < 0.01$  significant difference from control group.

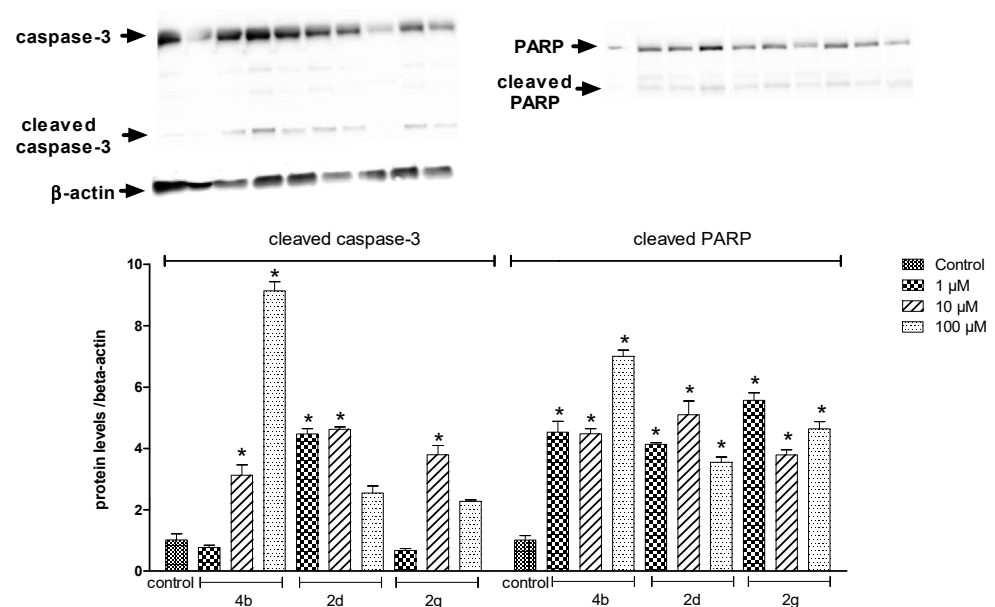


**Figure 5.** Changes in cleaved caspase-3 and cleaved PARP protein levels. Representative Western blots showing protein expressions of full-length or cleaved caspase-3 and PARP following treatments of compounds 2d, 2g and 4b at 3 concentrations (1, 10 and 100  $\mu$ M). Graphs indicate the relative densitometric values of the proteins. Quantification of protein product was performed by densitometric scanning. Data were normalized by using the  $\beta$ -actin signal and are expressed as arbitrary densitometric units. Values are means SD;  $n = 5$  in each group. \*  $p < 0.01$  significant difference from the control group.

Despite recent improvements in patient risk stratification and genetic profiling, neuroblastoma remains the most lethal extracranial solid tumor in children. The combination of chemotherapeutic drugs including cisplatin, doxorubicin, cyclophosphamide and vincristine results in therapeutic failure because of chemoresistance [37]. Therefore, any alternatives with therapeutic potential should be studied in detail. In the present study, the in vitro proapoptotic and antiproliferative activities of these selected compounds are promising for further structural modifications and may provide a useful template for the design of new antitumoral agents.

### 2.3. Molecular Modelling Studies

#### 2.3.1. Protein and Ligand Preparation

For docking studies, the 3D structure of the pro-apoptotic Bax protein was retrieved from the RCSB protein data bank using its PDB id: 1F16 [38]. This protein structure, which consists of 192 residues with 9 $\alpha$  helices without  $\beta$  sheets, was determined using the NMR solution technique. The 3D structure used was prepared by adding hydrogens, computing Gastiger charges, merging non-polar hydrogens and deleting water molecules. The preparation steps were carried out in the Bax protein by using the AutoDock Tools program (ADT) [39]. Further, the active site was selected to be around the  $\alpha$ 1 and  $\alpha$ 2 helices as being the most favorable pocket for the docking simulation.

#### 2.3.2. Molecular Docking Analysis

Molecular docking simulation was carried out with the pro-apoptotic Bax protein (1F16) and all ligands (i.e., pyrido-imidazole derivatives) using the AutoDock Vina software [40]. This tool functions using a Lamarckian Genetic Algorithm (LGA). The active site was input and the grid parameter file for the Bax protein was generated by fixing the number of grid points on the x = 4.528, y = -6.556, and z = -3.667 axes. AutoDock grids were calculated for regularly spaced points at intervals of 1.000 (Å) with dimensions of 30  $\times$  28  $\times$  22 (Å) and contained within a cube based on the helices  $\alpha$ 1 and  $\alpha$ 2 surrounding residues. The population size was set to 150. The maximum number of energy evaluations and generations was set to 500.000 and 1000, respectively. The rest of the docking parameters were set to the AutoDock Vina program default values. The LGA algorithm was used to find the best conformations in eight independent trials for each ligand.

To better understand whether or not the studied compounds had an effect on the activation of the Bax protein, molecular docking simulations of the three ligands (i.e., **2d**, **2g** and **4b**) with the  $\alpha$ 1 and  $\alpha$ 2 helices of the Bax trigger site were carried out. The simulations revealed that the ligands exhibit different and important types of interaction with significant docking scores (i.e., binding affinities). The interaction details of top three compounds with the active site residues are shown in Table 2.

**Table 2.** Most non bond interactions between Pro-apoptotic Bax protein and top 3 compounds.

Compound	Binding Free Energies (Kcal/mol)	Residues in Contact	Interaction Type	Distance in Å
<b>4b</b>	−6.9	Leu25	$\pi$ -sigma	3.89
		Pro49	$\pi$ -alkyl	4.65
		Pro51	$\pi$ -alkyl	4.34
		Gln52	$\pi$ -donor H-bond	3.95
		Asp53	$\pi$ -donor H-bond	4.16
<b>2d</b>	−6.7	Leu25	$\pi$ -sigma	3.74
		Pro49	$\pi$ -alkyl	4.03
		Pro51	$\pi$ -sigma	3.91
<b>2g</b>	−6.6	Leu25	$\pi$ -sigma	3.74
		Pro49	$\pi$ -sigma	3.56
		Pro51	$\pi$ -sigma	3.91

On the one hand, non-classical hydrogen bond (HB) and mixed/ $\pi$ -alkyl hydrophobic such as  $\pi$ -sigma,  $\pi$ -alkyl and  $\pi$ -donor H-bond interactions were found to have major effects in initiating the activation of the Bax protein. The examination of these types of interactions is illustrated in Figure 6. In this figure, green and pink regions indicate the areas where HB-acceptor and HB-donor areas are preferred, respectively. The main interacting amino acids were Leu25, Pro49 and Pro51 for the three docked ligands.

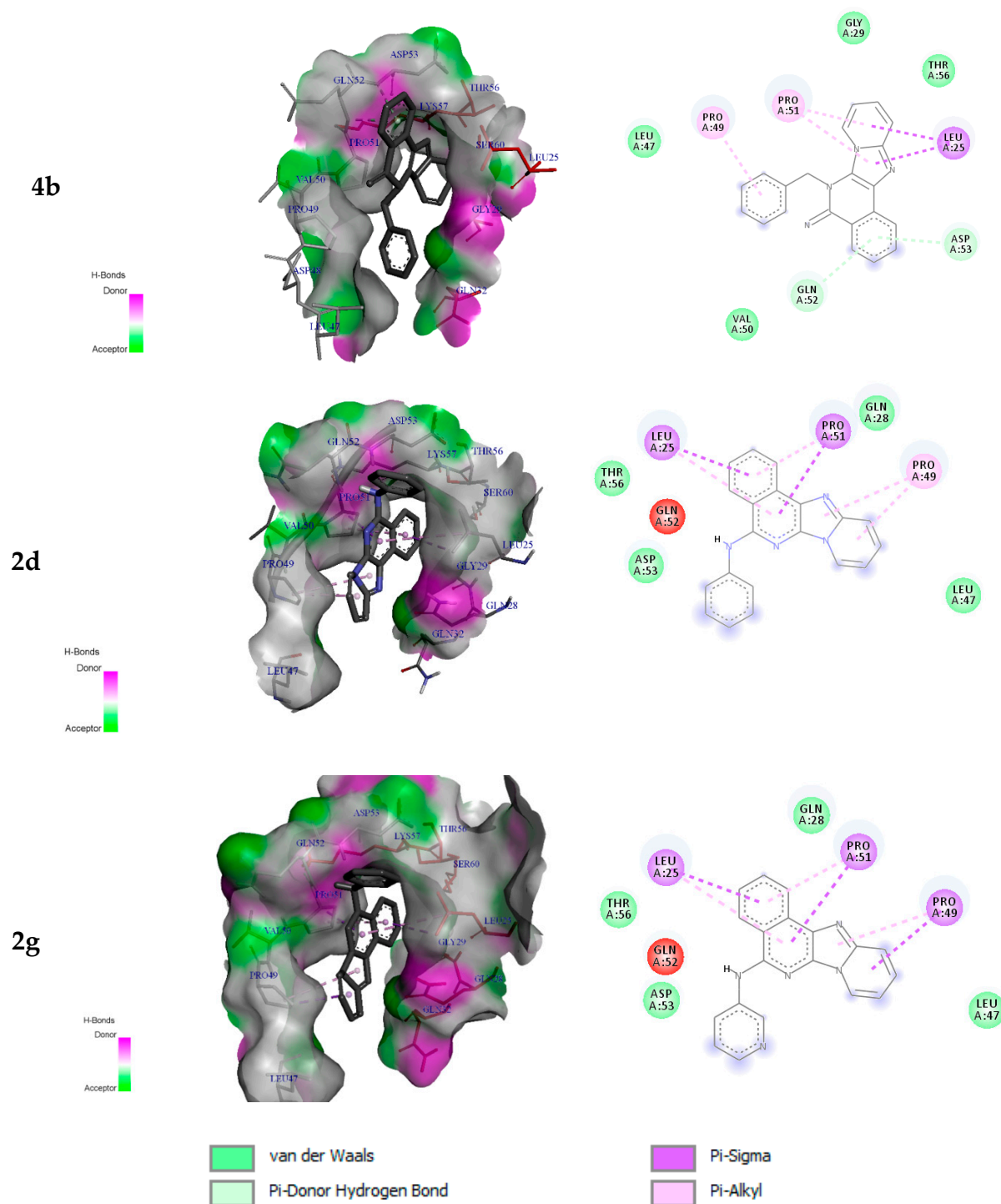


**Figure 6.** Hydrogen bond regions as exhibited by the active site (left). VDW and mixed/ $\pi$ -alkyl hydrophobic interactions (right) as exhibited by compounds 2d, 2g and 4b.

Additionally, both hydrophobic and hydrophilic amino acid residues of the active site groove played a contributing role in the interaction with the most active ligands (Figure 7). Indeed, the observed types of interactions of the selected compounds with the hydrophobic matrix of the active site could help in explaining the increase in the antiproliferative effect of these types of cells.

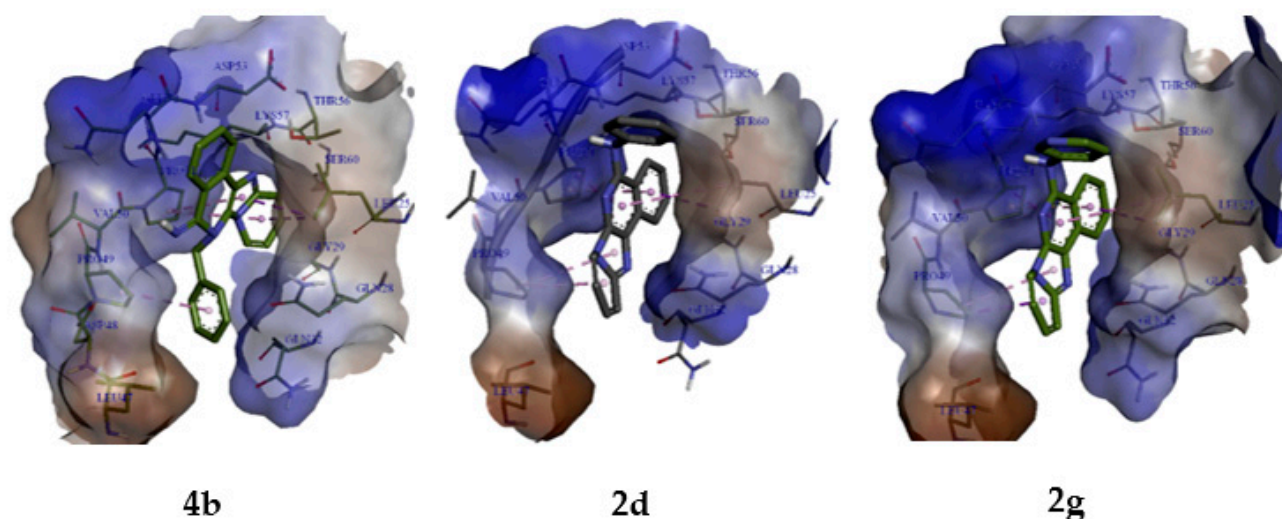


Figure 7. Hydrophobic area as exhibited by the active site along with compounds 2d, 2g and 4b.

All in all, it can be concluded that the initiation of Bax activation, which is taken away by the  $\alpha 1$ - $\alpha 2$  loop displacement, is due to exposure of the 12th to the 24th amino acid residues (Figure 8). As can be seen, the predicted model of Bax activation through displacement of the  $\alpha 1$ - $\alpha 2$  loop from a closed to an open conformation was induced by the selected compounds.

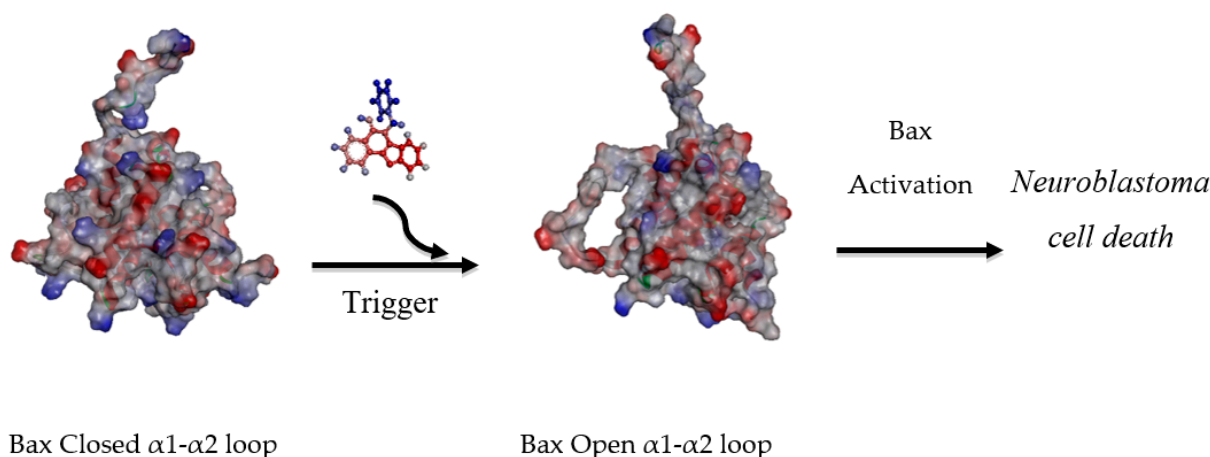


Figure 8. Predicted model of Bax activation initiated by displacement of the  $\alpha 1$ - $\alpha 2$  loop from a closed to an open conformation induced by the ligands examined in the present study.

### 3. Materials and Methods

#### 3.1. Chemistry Methods

##### 3.1.1. General Information

The reactions were monitored by thin-layer chromatography (TLC) analysis using silica gel (60 F254) plates. Compounds were visualized by UV irradiation. Flash column chromatography was performed on silica gel 60 (230–400.13 mesh, 0.040–0.063 mm). Melting points (mp ( $^{\circ}\text{C}$ )) were taken on samples in open capillary tubes and are uncorrected.

The infrared spectra of compounds were recorded on a Thermo Scientific Nicolet iS10 and are given in  $\text{cm}^{-1}$ .  $^1\text{H}$  and  $^{13}\text{C}$  NMR spectra were recorded on a Bruker DPX 250 MHz ( $^{13}\text{C}$ , 62.9 MHz), Bruker advance II 250.13 MHz ( $^{13}\text{C}$ , 63 MHz), Bruker advance 400.13 MHz ( $^{13}\text{C}$ , 101 MHz), or on a Bruker advance III HD nanobay 400.13 MHz ( $^{13}\text{C}$ , 101 MHz). Chemical shifts are given in parts per million from tetramethylsilane (TMS) as internal standard. Coupling constants (J) are reported in hertz (Hz). High-resolution mass spectra (HRMS) were performed on a Maxis Bruker 4G. The information is contained within Supplementary Material.

### 3.1.2. General Groebke–Blackburn–Bienaymé MCR Procedure for the Synthesis of (S1, S2 and S3)

To a solution of amine (1.06 mmol, 1 equiv) in 1 mL dichloromethane, 2-cyanobenzaldehyde (1.16 mmol, 1.1 equiv) and perchloric acid (2–3 drops, 70% in water) were added and left at room temperature for 1 h, then isonitrile (1.16 mmol, 1.1 equiv) was introduced. After completion of the reaction (controlled by TLC), the mixture was concentrated under reduced pressure and the crude material was purified by flash chromatography on silica gel to provide the expected product.

### 3.1.3. General N-Deprotection-cyclization Procedure

Compounds **1a–1j**, **3a** and **4a**, **4b** were prepared by following the N-deprotection-cyclization procedure, to a solution of **S1**, **S2** or **S3** (0.49 mmol, 1 equiv.) in dichloromethane (5 mL), TFA (5 mL) was added. After completion of the reaction (controlled by TLC), the mixture was concentrated and the residue was dissolved in water. The pH solution was adjusted at 8 and the resulting precipitate was collected by filtration, washed with water and dried. The crude product was purified by crystallization with  $\text{Et}_2\text{O}$ .

### 3.1.4. Buchwald–Hartwig Cross-Coupling Procedure

Compounds **2a–2j** and **3b** were prepared by following the Buchwald–Hartwig cross-coupling procedure [29]. Under argon atmosphere,  $\text{Pd}(\text{OAc})_2$  (2 mg, 0.0085 mmol, 0.02 equiv.), Xantphos (4,5-bis(diphenylphosphino)-9,9-dimethylxanthene) (5 mg, 0.0085 mmol, 0.02 equiv.) were introduced in a round-bottomed flask and diluted in dry toluene (1 mL) and left at room temperature for 1 h. Meanwhile, in a two-necked round-bottomed flask, aryl halide (0.426 mmol, 1.00 equiv.), **1(a–i)** or **3a** (100 mg, 0.426 mmol, 1.00 equiv.) and  $\text{Cs}_2\text{CO}_3$  (558 mg, 1.70 mmol, 4.00 equiv.) were introduced in dry toluene (5 mL). To this suspension, the previously pre-formed Pd-catalyst was added. The resulting mixture was flushed with argon and heated at 120 °C. After completion of the reaction (controlled by TLC), toluene was removed under reduced pressure, water (10 mL) was added and the resulting aqueous phase was extracted with ethyl acetate. The combined organic layer was dried over magnesium sulfate and concentrated under reduced pressure. The crude product was purified by flash chromatography on silica gel.

## 3.2. Biological Methods

### 3.2.1. Cell Culture and Treatments

The human neuroblastoma cell line (SH-SY5Y) used in this study was purchased from the American Type Culture Collection (ATCC, Catalog #CRL-2266, Manassas, VA, USA). Cells were suspended in complete Dulbecco's modified Eagle Medium (DMEM) (Life Technologies, Gibco BRL, Grand Island, NY, USA) supplemented with 10% fetal bovine serum (FBS, Hyclone, ATCC, Manassas, VA, USA), 1% penicillin and streptomycin (100 U/mL, Invitrogen, Fisher Scientific, Illkirch, France) and plated in cell culture dishes. The cultures were maintained at 37 °C in 5%  $\text{CO}_2$  95% humidified atmosphere. After reaching 85% confluence, cells were transferred to 96-well plates or culture dishes. For WST-1 experiments, cells were seeded into 96-well cell culture plates at a density of  $2 \times 10^3$  cells per well and allowed to adhere for 24 h. The culture medium was then replaced

with fresh medium containing compounds (100, 10, 1, 0.1  $\mu\text{M}$ ) and incubated in a 5%  $\text{CO}_2$  incubator.

For protein analysis, cells were seeded into 6-well cell culture plates at a density of  $0.5 \times 10^6$  cells/well and allowed to adhere to the surface for 24 h. The stock solutions of the test compounds (5 mM) were prepared in sterile DMSO and these stocks were then appropriately diluted with the complete culture medium and DMSO levels were maintained below 1% in the test concentrations.

### 3.2.2. Cell Proliferation Assay

SH-SY5Y cells were seeded at a density of  $2 \times 10^3$  cells/well into 96-well plates and incubated for 24 h. After 24 h, the cells were treated with the synthesized compounds at 0.1, 1, 10 and 100  $\mu\text{M}$  concentrations for 72 h. Following the 72 h exposure, the cell viability was determined using the WST-1 assay. Cell viability was evaluated using Cell Proliferation Reagent WST-1 (Roche, France) according to the manufacturer's instructions. The absorbance was measured at 440 nm and 600 nm using a microplate reader (VersaMax, Molecular Devices, USA). Percent survival was plotted relative to vehicle control cells, which were normalized to 100% survival. Culture medium with WST-1 without cells was used for background control.

### 3.2.3. Clonogenic Survival Assay

This assay is an *in vitro* cell survival and proliferation assay based on the ability of a single cell to grow into a colony [41–43]. Briefly, 1500 cells were mixed gently in 2 mL media and plated on a 6-well plate. After being incubated for 24 h, the drugs were applied. The media which contain drugs were refreshed weekly and cells were grown for 2 to 3 weeks. At the end, the cells were washed with phosphate-buffered saline and stained with 10% crystal violet. Colonies with a diameter of more than 50 cells were counted. The experiment was repeated three times.

### 3.2.4. Protein Analysis

SH-SY5Y cells ( $0.5 \times 10^6$  cell/well) were seeded into 6-well plates and incubated for 24 h. After 24 h, the cells were treated with the synthesized compounds at three different concentrations, 1, 10 and 100  $\mu\text{M}$  for 72 h. Following treatment, the cells were washed with ice-cold 1X PBS and lysed in 1X cell lysis buffer (phosphatase and protease inhibitors added). These lysates were quantified using the BCA protein assay. Then, Western blot assays were done by using cell lysates.

### 3.2.5. Western Blotting

Western blotting was performed by loading 30  $\mu\text{g}$  protein on 10% (*w/v*) tris-glycine denaturing gels and separating the proteins by electrophoresis, then transferring them to a PVDF membrane. After blocking, the membrane was incubated with primary antibodies, anti-PARP rabbit monoclonal antibody (1:1000, Cell Signaling Technology, Invitrogen Fisher Scientific, Illkirch, France), anti-caspase-3 rabbit monoclonal antibody (1:1000, Cell Signaling Technology), anti-Bax rabbit monoclonal antibody (1:1000, Cell Signaling Technology), anti-Bcl-2 rabbit monoclonal antibody (1:1000, Cell Signaling Technology) at +4 °C overnight. Following incubation, the membrane was incubated with anti- $\beta$ -actin mouse monoclonal antibody (1:1000, Cell Signaling Technology) at room temperature for 1 h. After washing, the membrane was incubated with infrared labeled secondary antibodies (Odyssey Western Blotting kit, LI-COR Biosciences, Lincoln, NE, USA) at room temperature for 1h. Proteins were visualized, and quantified by scanning the membrane on an Odyssey Infrared Imaging System (LI-COR Biosciences, Lincoln, NE, USA) with both 700- and 800-nm channels.

### 3.2.6. Statistical Analysis

Data were expressed as means  $\pm$  standard deviation (SD) for five or three independent experiments in triplicate. Comparisons of means between groups were performed by one-way analysis of variance (ANOVA) followed by Tukey's post hoc test.  $p < 0.05$  was considered statistically significant.

### 3.3. Computational Study

The 1F16 (Closed bax protein) [38] solution structure of a Pro-apoptotic Bax protein was prepared according to the protein preparation module in the AutoDockTools (ADT) package. Rigid and flexible conformations were prepared for all amino acids. Three-dimensional (3D) ligand structures were drawn and minimized using the Gaussview 05 and Gaussian programs [44], respectively. A semi-flexible docking study was performed with the AutoDock Vina program [40]. The best docking conformations of the compounds with the highest activities (i.e., **4b**, **2d** and **2g**) were selected to analyze different molecular interactions within the Bax protein active pocket using the Discovery studio program [45].

## 4. Conclusions

In summary, we report herein the design and synthesis of tetra-heterocycles functionalized by amine. The cytotoxic potential of these derivatives was evaluated in human neuroblastoma cell lines and showed moderate antiproliferative activity against the cancer cells with IC<sub>50</sub> values below 10  $\mu$ M for a few derivatives. The studies carried out have shown, on the one hand, that some compounds had a regulatory potential of apoptosis via control of the induction of mitochondrial dysfunction, and on the other hand, that these compounds had a potential to regulate the caspase 3 enzyme activation in a dose-dependent manner. These compounds enhance caspase-3 cleavage, thereby initiating the intrinsic apoptotic cascade. We show that the in vitro proapoptotic and antiproliferative activities of these selected compounds are promising for further structural modifications and may provide a useful template for the design of new antitumoral agents. Moreover, the molecular docking studies indicated that our synthetic derivatives have significant binding affinities with the target protein. As neuroblastoma is the most lethal extracranial solid tumor in children, any approaches with an interesting therapeutic potential should be studied in detail. The predicted model of Bax activation through displacement of the  $\alpha$ 1- $\alpha$ 2 loop from a closed to an open conformation (Figure 8) was induced by the selected compounds. Compounds **2d**, **2g** and **4b** possessed significant proapoptotic and antiproliferative activities and may be useful as lead molecules for designing new antitumoral agents.

**Supplementary Materials:** The following are available online at <https://www.mdpi.com/article/10.3390/ph14080750/s1>.

**Author Contributions:** Z.T., M.L., J.J., I.H., M.A.E., L.S., S.B.-R. and G.A.; validation, Z.T., M.L., J.J., I.H., M.A.E., L.S., S.B.-R. and G.A.; formal analysis, Z.T., M.L., J.J.; investigation, I.H., M.A.E., L.S., S.B.-R. and G.A.; resources, M.A.E., L.S., G.A. and S.B.-R.; data curation, Z.T., M.L., J.J., I.H., M.A.E., L.S., S.B.-R. and G.A.; writing—original draft preparation, Z.T., M.L.; writing—review and editing, M.A.E., L.S., G.A. and S.B.-R.; visualization, Z.T., M.L., J.J., I.H., M.A.E., L.S., S.B.-R. and G.A.; supervision, M.A.E., L.S., G.A. and S.B.-R.; project administration, M.A.E., L.S., G.A. and S.B.-R.; funding acquisition, M.A.E., L.S., G.A. and S.B.-R. All authors have read and agreed to the published version of the manuscript.

**Funding:** This research received no external funding.

**Institutional Review Board Statement:** Not applicable.

**Informed Consent Statement:** Not applicable.

**Data Availability Statement:** The chemical molecules studied in this article are described in reference [29] with the exception of products **4a** and **4b** which are described in Supplementary Material.

**Conflicts of Interest:** The authors declare no conflict of interest.

## References

1. Mueller, S.; Matthay, K.K. Neuroblastoma: Biology and staging. *Curr. Oncol. Rep.* **2009**, *11*, 431–438. [[CrossRef](#)]
2. Weinstein, J.L.; Katzenstein, H.M.; Cohn, S.L. Advances in the Diagnosis and Treatment of Neuroblastoma. *Oncologist* **2003**, *8*, 278–292. [[CrossRef](#)]
3. Colon, N.C.; Chung, D.H. Neuroblastoma. *Adv. Pediatr.* **2011**, *58*, 297–311. [[CrossRef](#)] [[PubMed](#)]
4. Johnsen, J.I.; Dyberg, C.; Wickström, M. Neuroblastoma—A Neural Crest Derived Embryonal Malignancy. *Front. Mol. Neurosci.* **2019**, *12*, 9. [[CrossRef](#)] [[PubMed](#)]
5. Yu, A.L.; Gilman, A.L.; Ozkaynak, M.F.; London, W.B.; Kreissman, S.G.; Chen, H.X.; Smith, M.; Anderson, B.; Villablanca, J.G.; Matthay, K.K.; et al. Anti-GD2 Antibody with GM-CSF, Interleukin-2, and Isotretinoin for Neuroblastoma. *N. Engl. J. Med.* **2010**, *363*, 1324–1334. [[CrossRef](#)] [[PubMed](#)]
6. Nile, D.L.; Rae, C.; Hyndman, I.J.; Gaze, M.N.; Mairs, R.J. An evaluation in vitro of PARP-1 inhibitors, rucaparib and olaparib, as radiosensitizers for the treatment of neuroblastoma. *BMC Cancer* **2016**, *16*, 621. [[CrossRef](#)] [[PubMed](#)]
7. Hanahan, D.; Weinberg, R.A. Hallmarks of cancer: The next generation. *Cell* **2011**, *144*, 646–674. [[CrossRef](#)]
8. Labi, V.; Erlacher, M. How cell death shapes cancer. *Cell Death Dis.* **2015**, *6*, e1675. [[CrossRef](#)] [[PubMed](#)]
9. Grosse, S.; Mathieu, V.; Pillard, C.; Massip, S.; Marchivie, M.; Jarry, C.; Bernard, P.; Kiss, R.; Guillaumet, G. New imidazo[1,2-*b*]pyrazoles as anticancer agents: Synthesis, biological evaluation and structure activity relationship analysis. *Eur. J. Med. Chem.* **2014**, *84*, 718–730. [[CrossRef](#)]
10. Baviskar, A.T.; Madaan, C.; Preet, R.; Mohapatra, P.; Jain, V.; Agarwal, A.; Guchhait, S.K.; Kundu, C.N.; Banerjee, U.C.; Bharatam, P.V. N-Fused Imidazoles As Novel Anticancer Agents That Inhibit Catalytic Activity of Topoisomerase II $\alpha$  and Induce Apoptosis in G1/S Phase. *J. Med. Chem.* **2011**, *54*, 5013–5030. [[CrossRef](#)]
11. Guchhait, S.K.; Chaudhary, V. Desilylative activation of TMSCN in chemoselective Strecker-Ugi type reaction: Functional fused imidazoles as building blocks as an entry route to annulated purines. *Org. Biomol. Chem.* **2014**, *12*, 6694–6705. [[CrossRef](#)] [[PubMed](#)]
12. Marzouk, V.H.R.; Hennum, M.; Gundersen, L.L. Efficient synthesis of cytotoxic pyrido[1,2-*e*]purines from purines employing direct C-allylation and RCM-oxidation as key steps. *Tetrahedron Lett.* **2013**, *54*, 3437–3439. [[CrossRef](#)]
13. Favier, A.; Blackledge, M.; Simorre, J.P.; Crouzy, S.; Dabouis, V.; Gueiffier, A.; Marion, D.; Debouzy, J.C. Solution structure of 2-(pyrido[1,2-*e*]purin-4-yl)amino-ethanol intercalated in the DNA duplex d(CGATCG)<sub>2</sub>. *Biochemistry* **2001**, *40*, 8717–8726. [[CrossRef](#)]
14. Debouzy, J.C.; Gueiffier, A.; Fauvelle, F.; Viols, H.; Dejean, E.; Neirinck, V.; Peinnequin, A.; Bachelet, C.; Perly, B.; Chapat, J.P. Synthetic pyridopurines derived from food pyrolysis products: Intercalation, interactions with membranes, cyclodextrin complexation, and biological mitogenic properties. *J. Pharm. Sci.* **1996**, *85*, 200–205. [[CrossRef](#)] [[PubMed](#)]
15. Brullo, C.; Spisani, S.; Selvatici, R.; Bruno, O. N-Aryl-2-phenyl-2,3-dihydro-imidazo[1,2-*b*]pyrazole-1-carboxamides 7-substituted strongly inhibiting both fMLP-OME- and IL-8-induced human neutrophil chemotaxis. *Eur. J. Med. Chem.* **2012**, *47*, 573–579. [[CrossRef](#)] [[PubMed](#)]
16. Bruno, O.; Brullo, C.; Bondavalli, F.; Ranise, A.; Schenone, S.; Falzarano, M.S.; Varani, K.; Spisani, S. 2-Phenyl-2,3-dihydro-1*H*-imidazo[1,2-*b*]pyrazole derivatives: New potent inhibitors of fMLP-induced neutrophil chemotaxis. *Bioorganic Med. Chem. Lett.* **2007**, *17*, 3696–3701. [[CrossRef](#)]
17. Tyagi, V.; Khan, S.; Bajpai, V.; Gauniyal, H.M.; Kumar, B.; Chauhan, P.M.S. Skeletal diverse synthesis of N-fused polycyclic heterocycles via the sequence of Ugi-type MCR and CuI-catalyzed coupling/tandem Pictet-Spengler reaction. *J. Org. Chem.* **2012**, *77*, 1414–1421. [[CrossRef](#)]
18. Deady, L.W.; Rodemann, T. Reduced Benzimidazo[2,1-*a*]isoquinolines. Synthesis and Cytotoxicity Studies. *Aust. J. Chem.* **2001**, *54*, 529–534. [[CrossRef](#)]
19. Vanotti, E.; Fiorentini, F.; Villa, M. Synthesis of novel derivatives of 1*H*-imidazo[1,2-*b*]pyrazole as potential CNS-agents. *J. Heterocycl. Chem.* **1994**, *31*, 737–743. [[CrossRef](#)]
20. Reddyrajula, R.; Dalimba, U.K. Structural modification of zolpidem led to potent antimicrobial activity in imidazo[1,2-*a*]pyridine/pyrimidine-1,2,3-triazoles. *New J. Chem.* **2019**, *43*, 16281–16299. [[CrossRef](#)]
21. Guetzoyan, L.; Nikbin, N.; Baxendale, I.R.; Ley, S.V. Flow chemistry synthesis of zolpidem, alpidem and other GABAA agonists and their biological evaluation through the use of in-line frontal affinity chromatography. *Chem. Sci.* **2013**, *4*, 764–769. [[CrossRef](#)]
22. Arnould, M.; Hiebel, M.A.; Massip, S.; Léger, J.M.; Jarry, C.; Berteina-Raboin, S.; Guillaumet, G. Efficient Metal-Free Synthesis of Various Pyrido[2',1':2,3]imidazo[4,5-*b*]quinolines. *Chem. Eur. J.* **2013**, *19*, 12249–12253. [[CrossRef](#)] [[PubMed](#)]
23. Bonjean, K.; De Pauw-Gillet, M.C.; Defresne, M.P.; Colson, P.; Houssier, C.; Dassonneville, L.; Bailly, C.; Greimers, R.; Wright, C.; Quetin-Leclercq, J.; et al. The DNA Intercalating Alkaloid cryptolepine Interferes with Topoisomerase II and Inhibits Primarily DNA Synthesis in B16 Melanoma Cells. *Biochemistry* **1998**, *37*, 5136–5146. [[CrossRef](#)] [[PubMed](#)]
24. Arzel, E.; Rocca, P.; Grellier, P.; Labaëid, M.; Frappier, F.; Gueritte, F.; Gaspard, C.; Marsais, F.; Godard, A.; Quéguiner, G. New Synthesis of Benzo- $\delta$ -carbolines, Cryptolepines and their Salts: In vitro Cytotoxic, Antiplasmodial and Antitrypanosomal Activities of  $\delta$ -Carbolines, Benzo- $\delta$ -carbolines and Cryptolepines. *J. Med. Chem.* **2001**, *44*, 949–960. [[CrossRef](#)] [[PubMed](#)]

25. Chewonarin, T.; Kinouchi, T.; Kataoka, K.; Arimochi, H.; Kuwahara, T.; Vinitketkumnuen, T.; Ohnishi, T. Effects of roselle (*Hibiscus sabdariffa* Linn.), a Thai medicinal plant, on the mutagenicity of various known mutagens in salmonella typhimurium and of formation of Aberrant Crypt Foci Induced by a Colon Carcinogen Azoxymethane and 2-amino-1-methyl-6-phenylimidazo[4,5-*b*]pyridine in F344 rats. *Food Chem. Toxicol.* **1999**, *37*, 591–601. [[CrossRef](#)]
26. Groebke, K.; Weber, L.; Mehlin, F. Synthesis of Imidazo[1,2-*a*]annulated Pyridines, Pyrazines and Pyrimidines by a novel Three-Component Condensation. *Synlett* **1998**, *1998*, 661–663. [[CrossRef](#)]
27. Blackburn, F.; Guan, B.; Fleming, P.; Shiosaki, K.; Tsai, S. Parallel synthesis of 3-aminoimidazo[1,2-*a*]pyridines and pyrazines by a new Three-Component Condensation. *Tetrahedron Lett.* **1998**, *39*, 3635–3638. [[CrossRef](#)]
28. Bienaymé, H.; Bouzid, K. A New Heterocyclic Multicomponent Reaction for the Combinatorial Synthesis of Fused 3-Aminoimidazoles. *Angew. Chem. Int. Ed.* **1998**, *37*, 2234–2237. [[CrossRef](#)]
29. Tber, Z.; Hiebel, M.A.; Allouchi, H.; El Hakmaoui, A.; Akssira, M.; Guillaumet, G.; Berteina-Raboin, S. Metal free direct formation of various substituted pyrido[2',1':2,3]imidazo[4,5-*c*]isoquinolin-5-amines and their further functionalization. *RSC Adv.* **2015**, *5*, 35201–35210. [[CrossRef](#)]
30. Ruiz-Castillo, P.; Buchwald, S.L. Applications of Palladium-Catalyzed C-N Cross-Coupling Reactions. *Chem. Rev.* **2016**, *116*, 12564–12649. [[CrossRef](#)]
31. Loubidi, M.; Lorion, M.; El Hakmaoui, A.; Bernard, P.; Akssira, M.; Guillaumet, G. One-Step Synthesis of 1H-Imidazo[1,5-*a*]imidazole Scaffolds and Access to their Polyheterocycles. *Synthesis* **2019**, *51*, 3973–3980. [[CrossRef](#)]
32. Sugimoto, T.; Jin, H.; Fijita, M.; Fukunaga, T.; Nagaoka, N.; Yamaai, T.; Ichikawa, H. Induction of activated caspase-3 immunoreactivity and apoptosis in the trigeminal ganglion neurons by neonatal peripheral nerve injury. *Brain Res.* **2004**, *1017*, 238–243. [[CrossRef](#)]
33. Ten Berge, R.L.; Meijer, C.J.L.M.; Dukers, D.F.; Alain Kummer, J.; Bladergroen, B.A.; Vos, W.; Erik Hack, C.; Ossenkoppele, G.J.; Oudejans, J.J. Expression levels of apoptosis-related proteins predict clinical outcome in anaplastic large cell lymphoma. *Blood* **2002**, *99*, 4540–4546. [[CrossRef](#)]
34. Newman, E.A.; Lu, F.; Bashllari, D.; Wang, L.; Opihari, A.W.; Castle, V.P. Alternative NHEJ pathway components are therapeutic targets in high-risk neuroblastoma. *Mol. Cancer Res.* **2005**, *13*, 470–482. [[CrossRef](#)]
35. Kaufmann, S.H.; Desnoyers, S.; Ottaviano, Y.; Davidson, N.E.; Poirier, G.G. Specific Proteolytic Cleavage of Poly(ADP-ribose) Polymerase: An Early Marker of Chemotherapy-induced Apoptosis. *Cancer Res.* **1993**, *53*, 3976–3985. [[PubMed](#)]
36. Nicholson, D.W.; Ali, A.; Thornberry, N.A.; Vaillancourt, J.P.; Ding, C.K.; Gallant, M.; Gareau, Y.; Griffin, P.R.; Labelle, M.; Lazebnik, Y.A.; et al. Identification and inhibition of the ICE/CED-3 protease necessary for mammalian apoptosis. *Nature* **1995**, *376*, 37–43. [[CrossRef](#)]
37. Cheung, N.K.V.; Dyer, M.A. Neuroblastoma: Developmental biology, cancer genomics and immunotherapy. *Nat. Rev. Cancer* **2013**, *13*, 397–411. [[CrossRef](#)]
38. Suzuki, M.; Youle, R.J.; Tjandra, N. Structure of bax: Coregulation of dimer formation and intracellular localization. *Cell* **2000**, *103*, 645–654. [[CrossRef](#)]
39. Morris, G.M.; Ruth, H.; Lindstrom, W.; Sanner, M.F.; Belew, R.K.; Goodsell, D.S.; Olson, A.J. Software news and updates AutoDock4 and AutoDockTools4: Automated docking with selective receptor flexibility. *J. Comput. Chem.* **2009**, *30*, 2785–2791. [[CrossRef](#)] [[PubMed](#)]
40. Trott, O.; Olson, A.J. AutoDock Vina: Improving the speed and accuracy of docking with a new scoring function, efficient optimization, and multithreading. *J. Comput. Chem.* **2009**, *31*, 455–461. [[CrossRef](#)]
41. Plumb, J.A. Cell sensitivity assays: Clonogenic assay. *Methods Mol. Med.* **2004**, *88*, 159–164. [[CrossRef](#)] [[PubMed](#)]
42. Ozpolat, B.; Akar, U.; Mehta, K.; Lopei-Berestein, G. PKC $\delta$  and tissue transglutaminase are novel inhibitors of autophagy in pancreatic cancer cells. *Autophagy* **2007**, *3*, 480–483. [[CrossRef](#)] [[PubMed](#)]
43. Tekedereli, I.; Alpay, S.N.; Tavares, C.D.J.; Cobanoglu, Z.E.; Kaoud, T.S.; Sahin, I.; Sood, A.K.; Lopez-Berestein, G.; Dalby, K.N.; Ozpolat, B. Targeted Silencing of Elongation Factor 2 Kinase Suppresses Growth and Sensitizes Tumors to Doxorubicin in an Orthotopic Model of Breast Cancer. *PLoS ONE* **2012**, *7*, e41171. [[CrossRef](#)] [[PubMed](#)]
44. Frisch, M.J.; Trucks, G.W.; Schlegel, H.B.; Scuseria, G.E.; Robb, M.A.; Cheeseman, J.R.; Scalmani, G.; Barone, V.; Mennucci, B.; Petersson, G.A.; et al. *Gaussian 09, Revision B.01*; Gaussian Inc.: Wallingford, CT, USA, 2009. Available online: <http://gaussian.com/> (accessed on 1 November 2016).
45. Systèmes, B.D. Discovery Studio Modeling Environment, San Diego Dassault Systèmes. (n.d.). Available online: <http://accelrys.com/products/collaborative-science/biovia-discovery-studio/> (accessed on 15 April 2018).